Computational Particle Mechanics (2021) 8:1089–1101
https://doi.org/10.1007/s40571-020-00355-0

Multiscale modeling of continuous crushing of granular media: the role of grain microstructure

Fan Zhu[1] · **Jidong Zhao**[1]

Received: 20 November 2019 / Revised: 24 June 2020 / Accepted: 26 August 2020 / Published online: 8 September 2020

Abstract
Natural granular materials such as sands often possess complex microstructural features including cleavage and minerals interfaces. Those features bring apparent mechanical anisotropy to particles and are known to have pronounced influence on particle crushing characteristics. This paper presents a multiscale simulation of continuous crushing of granular sand under one-dimensional compression in consideration of particle-scale anisotropy through modeling planes of weakness inside individual particles, with reference to granular materials rich in minerals and containing cleavages. The multiscale modeling is based on a coupled peridynamics and non-smooth contact dynamics method where peridynamics is used to model crushing of individual particles and non-smooth contact dynamics is employed to simulate discrete granular system. Weak microstructural planes are simulated by breaking a fraction of peridynamic bonds as an initial condition. Simulation results show that anisotropic particles containing weak planes result in larger number of fragments and exhibit relatively higher fractal dimension with respect to particle size. Particle shape is found to approach a steady state profile with continuous crushing. Anisotropic particles generally bear smaller sphericity, aspect ratio, elongation and flatness than those isotropic particles. The anisotropy in particles seems to mitigate shape effect on particle strength and crushing energy. Macromechanical yield stress of the sample is related to single particle strength monotonically, but the relationship appears to be nonlinear when different microstructural features are involved.

Keywords Weak plane · Particle crushing · Particle shape · Strength · Multiscale modeling

1 Introduction

Particle crushing is a fundamental physical process underlying many macromechanical behaviors of granular materials. It has great relevance to many fields including geotechnical, mining, pharmaceutical and chemical industries where crushable granular materials are routinely handled. Large efforts have been devoted to developing advanced numerical tools for realistic simulation of particle crushing and understanding the underlying physics. Particle crushing in granular media by its nature involves complex, multiscale physics. On a mesoscale or representative elementary volume scale, the material can be characterized as a discrete granular system, whereas on particle scale, the material is usually of continuum nature where various microstructural features may be present and affect fracturing process. Granular materials, and particularly natural sands and rocks, often possess complex microstructural features such as cleavage and mineral boundaries [1], surface flaws [2], microcracks [3] and bedding structures [4] depending on mineralogy, purity and formation history. In particular, cleavage is a common feature in many minerals such as feldspar and mica in the form of crystallographic structural planes along which fracture may easily develop under shear or tension. Those weak structural planes bring apparent mechanical anisotropy to the particle. The strength, location and orientation of the weak planes affect crushing load and fracture pattern of a particle [1, 5, 6]. Figure 1 illustrates crushing of a granite sand particle where fractures develop along mineral cleavage [1]. It can be expected that those particle-scale features may subsequently affect gradation, morphology and macroscopic strength–strain relations of the granular material. Incorporation of those particle-scale features into numerical modeling is demanded for realistic simulation and investigation of

✉ Fan Zhu
fzhuaa@connect.ust.hk

[1] Department of Civil and Environmental Engineering, The Hong Kong University of Science and Technology, Hong Kong, SAR, China

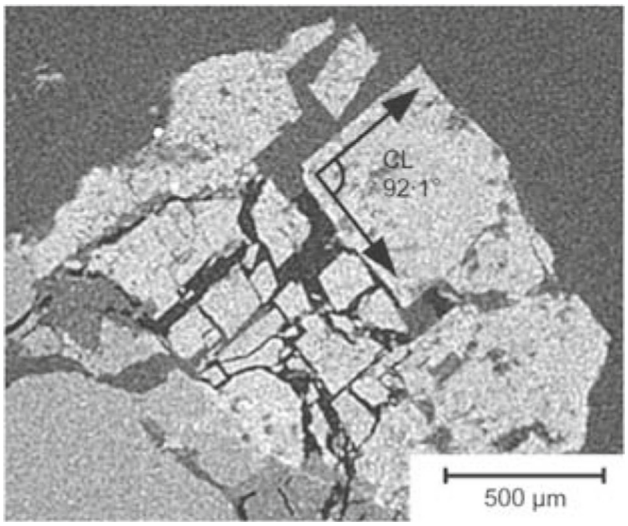

Fig. 1 Fracture pattern of a granite sand particle [1]. Cracks at right angles following the cleavage of feldspar are observed

microstructural behaviors of crushable granular materials for which past study has been limited. A common approach to model the particle-scale features is to employ a discrete-based method such as discrete element method (DEM) [7] or contact dynamics [8], where each breakable particle is simulated by bonded clump of spheres [9–12] or other elements such as tetrahedron and polygon/polyhedron [13–16]. The mechanical anisotropy can be modeled with proper assignment of bonds between the elements, and such approach has been commonly used for analyzing anisotropic rocks [17, 18]. For large granular system subject to continuous particle crushing, the bonded element approach may nonetheless be computationally overwhelming. Alternatively, the particle-scale features may be implemented under a multiscale modeling framework, where crushing of individual particles is explicitly modeled with a continuum approach such as finite element method or peridynamics [19–21].

In this paper, we present numerical modeling for mechanically anisotropic sands subject to continuous particle crushing process where particle-scale weak planes are considered explicitly. The modeling approach is embedded in a recently developed multiscale computational framework using combined peridynamics (PD) and non-smooth contact dynamics methods (NSCD) [21]. Crushing of particles is analyzed with PD, and the planes of weakness are modeled by setting a fraction of peridynamic bonds broken as an initial condition. The weak planes are modeled recursively in all particles including the fragmented pieces to represent intrinsic structural features commonly observed in minerals with cleavage structure. Simulations are presented for isotropic particles and anisotropic particles containing single weak plane and three orthogonal weak planes. With that, a study is carried out to examine effect of the particle-scale anisotropy on particle size and shape evolution, particle strength as well as crushing energy.

2 Computational approach

2.1 Peridynamic modeling of particle crushing

The PD method [22, 23] is employed to simulate crushing of individual particles. The method is a material point-based, non-local method known to be suitable for modeling fracture-related problems in continuum media. It was applied in modeling fracturing in many brittle materials such as glass [24], ceramics [25] and sand particle [26]. In PD, a continuum domain is represented by discretized material points and interactions are established between pairs of points through peridynamic bonds. The early stage, bond-based PD theory assumes that bond force only acts along the bond direction and is independent of neighboring conditions. The theory is applicable to limited type of materials. The later developed, state-based PD permits the bond force to act along the bond direction (ordinary type) or not (non-ordinary type) with consideration of neighborhood conditions. Various types of material models can be implemented in state-based PD. In this study, we employ the ordinary-type state-based peridynamics theory [23] as implemented in an open-source code *Peridigm* [27] for PD computations. The basic equation of motion writes:

$$\rho(\boldsymbol{x})\,\ddot{\boldsymbol{u}}(\boldsymbol{x},t) = \int_{\Omega_x}\left[\boldsymbol{T}(\boldsymbol{x},t)\langle\boldsymbol{x}'-\boldsymbol{x}\rangle - \boldsymbol{T}(\boldsymbol{x}',t)\langle\boldsymbol{x}-\boldsymbol{x}'\rangle\right]dV_{x'} + \boldsymbol{b}(\boldsymbol{x},t) \tag{1}$$

where $\boldsymbol{x}$ represents a material point, ρ denotes material density, $\boldsymbol{u}$ represents displacement and $\boldsymbol{b}$ denotes body force density. A material point is assumed to interact with other material points (i.e., neighboring points) within a domain represented by $\boldsymbol{\Omega}_x$ which is often termed *family* of $\boldsymbol{x}$. $dV_{x'}$ represents volume of a neighboring material point $\boldsymbol{x}'$. $\boldsymbol{T}$ represents a force state which maps deformation between two material points into peridynamic bond force density. A variety of material models may be implemented through the force state. A linear peridynamic solid (LPS) material model [27], which is a non-local analogy to the linear elastic material model, is applied to simulate crushing of elastic brittle particles. The same model was applied for modeling crushing of sand particles in a previous study [26]. The force state $\boldsymbol{T}$ is calculated by

$$\boldsymbol{T} = \left(\frac{3K\theta\langle\boldsymbol{x}\rangle}{m\langle\boldsymbol{x}\rangle}\omega\underline{x} + \frac{15\mu}{m\langle\boldsymbol{x}\rangle}\omega\underline{e}^{d}\right)\frac{\boldsymbol{Y}}{||\boldsymbol{Y}||} \tag{2}$$

where μ and K denote the shear and bulk modulus, respectively. ω is an influence function which is taken to be one in the simulation. θ represents dilatation at a material point. m is a weighted volume, and $\underline{x}$ equals the length of the bond. $\boldsymbol{Y}$ represents the deformed bond vector, and the term $\boldsymbol{Y}/||\boldsymbol{Y}||$ ensures that the bond force acts along the bond direction. The dilatation and weighted volume at a material point are calculated by

$$\theta\langle \boldsymbol{x}\rangle = \frac{3}{m\langle \boldsymbol{x}\rangle}\int_{\Omega_x} \omega||\boldsymbol{\xi}||\underline{e}dV_{x'} \tag{3}$$

$$m\langle \boldsymbol{x}\rangle = \int_{\Omega_x} \omega||\boldsymbol{\xi}||^2 dV_{x'} \tag{4}$$

where $\underline{e}$ represents the scalar bond extension from the initial state $\boldsymbol{\xi}$. It consists of an isotropic part $\underline{e}^i$, calculated by $\theta\langle \boldsymbol{x}\rangle \underline{x}/3$, and a deviatoric part calculated by $\underline{e} - \underline{e}^i$.

Initiation and propagation of cracks are modeled by allowing the peridynamic bonds to break. A critical stretch damage model [28] is applied. It assumes that a bond will break if its strain reaches a critical level, s_c, calculated by:

$$s_c = \sqrt{G_c/\left[\left(3\mu + \left(\frac{3}{4}\right)^4\left(K - \frac{5\mu}{3}\right)\right)\delta\right]} \tag{5}$$

where G_c represents critical energy release rate of the material. δ is referred to as *horizon*—a radius defining the *family* of a material point, and it is selected to be three times the discretized element size following a common practice in PD modeling. In the presented simulations, each particle is uniformly discretized following a cubic pattern and the element size refers to the distance between neighboring material points. The modeled element size is about $0.06d$ where d is the diameter of a sphere having the same volume to the particle. This leads to approximately 2500 discretized material points for each particle. Breakage of bonds is irreversible, meaning that once a bond is broken, it will no longer carry any force and the force that was originally borne on it will be redistributed to its neighboring bonds. Such process may result in successive breakage of bonds and eventually form fracture surfaces.

To assess location of fractures in a continuum domain, a parameter *damage* is defined at each material point by

$$\varphi\langle \boldsymbol{x}\rangle = 1 - \frac{\int_{\boldsymbol{\Omega}_x} g\langle \boldsymbol{\xi}\rangle dV_{\boldsymbol{x}'}}{\int_{\boldsymbol{\Omega}_x} dV_{\boldsymbol{x}'}} \tag{6}$$

where $g\langle \boldsymbol{\xi}\rangle$ denotes damage of a bond $\boldsymbol{\xi}$ in the neighborhood of $\boldsymbol{x}$. g equals one for an intact bond and zero for a broken bond. Consequently, the damage φ ranges between zero and unity and higher φ indicates more broken bonds. Damage of material points is used to trace the location and propagation of cracks in a continuum media.

2.2 Modeling planes of weakness

Planes of weakness reflect intrinsic structural features of a crystalline material. The strength at the planes of weakness decides degree of strength anisotropy of a particle. In rock mechanics, such anisotropicity is often assessed with a disk Brazilian test where a disk specimen is diametrically compressed until broken. The strength of the specimen is dependent of the strength and orientation of the weak planes. For rock specimens with layered structure, the maximum strength is obtained when the orientation of the weak planes is or about perpendicular to the loading direction, whereas the minimum strength is spotted when the orientation of the weak planes is or near parallel to the loading direction [29–31]. The ratio between the minimum and maximum strengths indicates the strength anisotropy of the rock specimen and was found to range typically between 0.3 and 0.7 for a wide variety of rocks [5]. Such test is however uncommon for sand particles.

To simulate the planes of weakness, a modification is made to the damage model in PD by randomly setting a fraction, as denoted by η, of the bonds that cross the selected planes to be broken at the beginning of simulation. Technically, this is done by drawing a random number between 0 and 1 for each bond crossing the plane and if the number is less than η, the bond is set to be broken. The fraction of broken bonds determines the strength against fracture at the weak plane. Setting η to zero renders intact material without plane of weakness, while setting η to unity creates a pre-defined crack. Selecting a proper η requires knowledge on the specific material to be simulated and calibration with particle crushing test results. Two sets of parametric studies are performed to assess the relation between η and the degree of strength anisotropy. A disk specimen with a diameter-to-thickness ratio of 2:1 and a sphere specimen are simulated with a single weak plane crossing center of the specimen modeled parallel and perpendicular to the loading direction (which gives the minimum and maximum strength of the particle). The ratio of minimum and maximum failure load versus η is summarized in Fig. 2. In this study, we select η to be 0.7 for the modeled sand particles, which corresponds to a min/max strength ratio of at least 0.5 to 0.6 for both disk and sphere. The ratio could be larger when the weak plane is not modeled through the center of the particle. Figure 3 illustrates a spherical particle modeled in PD containing a single weak plane with $\eta = 0.7$ and oriented perpendicular and parallel to the loading which is applied diametrically along the vertical direction. The modeled weak plane represents a zone where the initial damage of material is greater than zero. Cracks are seen to develop along the modeled weak plane in both cases. The for-

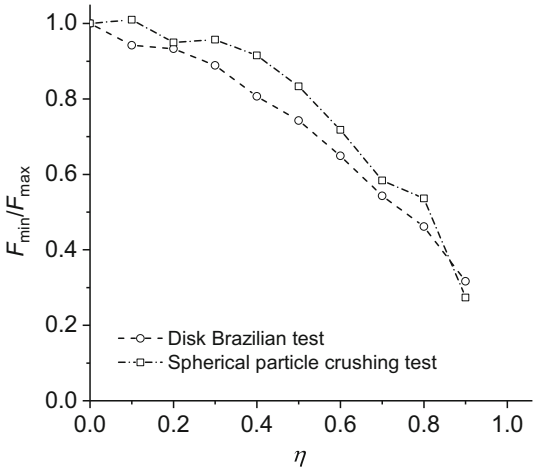

Fig. 2 The relation between η and strength anisotropy for disk Brazilian test and single spherical particle crushing test. η indicates the fraction of peridynamic bonds set to be broken at weak plane

mer case results in four slice-pattern fragments, whereas the latter case leads to eight pieces of fragments whose shape is distinct from the former case. The illustration implies potentially large influence of weak planes on fracture pattern of particles. It is worth mentioning that the weak planes can be modeled in different ways. An alternative approach to the one described above is to assign smaller critical energy release rates at the weak planes, and this will subsequently lead to smaller critical stretch values being assigned to the bonds crossing the weak planes.

For each grain, only one weak plane is modeled per orientation with a purpose to reflect anisotropy in the grain while controlling computational cost. For example, a single weak plane is modeled at a randomly selected location in the particle to represent a layered structure. Three weak planes are modeled along three orthogonal directions for particles with orthogonal cleavage structure. The location of the weak plane is selected within the particle at a random location along its orientation axis. The orientation axis refers to an axis crossing the center of the particle while paralleling with the pre-defined normal direction of the weak plane. Theoretically, one may simulate multiple weak planes with different strengths to gain better realisticity. However, due to the non-local nature of PD, setting pre-defined broken bonds has influence over the horizon of relevant material points (e.g., three times element size). Hence if two or more weak planes are closely spaced, unwanted interdependency may develop among the planes unless a finer discretization is adopted which incurs higher computational cost. The modeled weak planes are assumed to be crossing the body, while it is acknowledged that multiple types of minerals may present even in a single particle and render much complex patterns of crystallographic structural planes. Orientations of the weak planes are carried with the particle during simulation. When a particle breaks, new weak planes are modeled in the child particles following the same procedures described earlier. Modeling weak planes in the child particles inherits the anisotropicity in the parent particle. The anisotropicity is due to cleavage in minerals which originate from atomic lattice structure and thus exist even at very small scales, for example, on a length scale of micrometer [32]. The orientation of the weak planes for the child particles is set to be the same as that in the parent particle before breakage. Such modeling process is schematically illustrated in Fig. 4.

2.3 Multiscale modeling of granular system

Using peridynamics alone to simulate discrete granular system encounters computational efficiency issues when handling large amount of 3D objects [33] owing to the low efficiency of material point-based contact detection and modeling. To address such issue, we employ a recently developed multiscale modeling framework based on combined PD and NSCD [21] where rigid body motions and particle interactions are fully handled by NSCD and crushing of individual particles is analyzed by PD. The framework utilizes advantages of both computational tools to maximize computational efficiency while preserving realisticity of the simulation. Computational scheme of the multiscale modeling framework is shown in Fig. 5, and interested readers are referred to a previous work [21] for further details. The simulation

Fig. 3 Particles with single weak plane modeled in PD analysis before and after breakage: **a** one weak plane along loading direction; **b** one weak plane perpendicular to loading direction

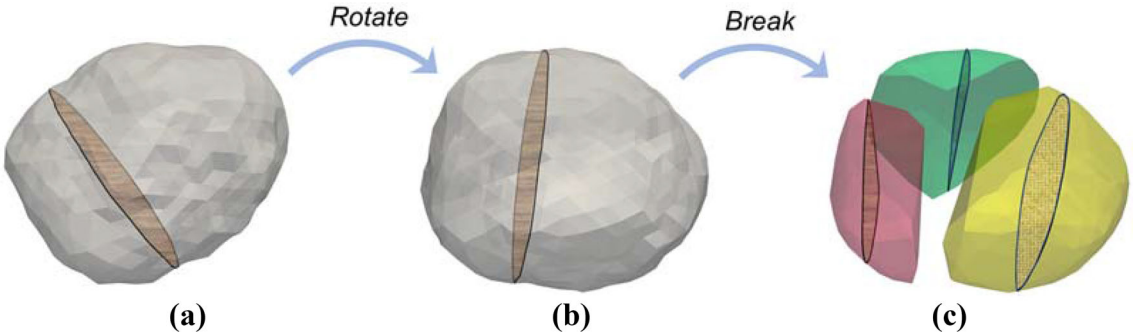

Fig. 4 Schematic illustration of modeling of weak planes: **a** Orientation of a weak plane is assigned; **b** orientation of the weak plane is carried with the rotation of particle; **c** after breakage, weak planes with the same orientation are assigned to child particles

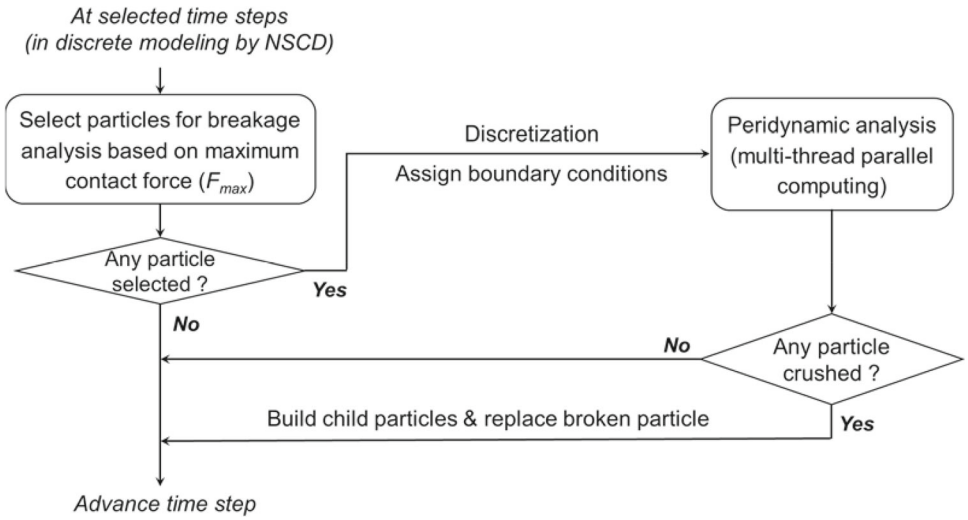

Fig. 5 Multiscale computational scheme for granular material with consideration of particle crushing

procedures can generally be described by three major stages. *First*, at designated time steps in discrete modeling, particles are screened for breakage analysis based on a maximum contact force ($F_{\max}$) criterion. Those with $F_{\max}$ exceeding a threshold are selected for breakage analysis. *Second*, PD analyses are performed to each selected particle. In the PD model, each particle is discretized into approximately 2500 material points and the contact force is applied to a contact zone defined as twice the element size in PD discretization. Multi-thread parallel computing is implemented to speed up the computation. *Third*, for particles that undergo crushing, the geometry of child particles will be built with either convex or concave polyhedrons and the original particle will be replaced in discrete modeling. With a balanced consideration between computational cost and accuracy on particle shape description, all broken pieces with equivalent diameter less than 0.8 mm or convexity more than 0.85 are described by convex polyhedrons. The convexity is defined as the volume of the particle divided by the volume of the minimum convex polyhedron enclosing the particle. In the presented simulations, open-source code *Project Chrono* [34] is used for NSCD-based discrete modeling and *Computational Geometry Algorithms Library* [35] is employed to aid geometrical computations.

3 Simulation of 1-D compression

3.1 Model setup

The simulated sample consists of initially 510 spherical particles with diameters ranging from 1.5 to 1.7 mm, placed in a cylinder-like smooth container having a diameter of 20 mm. The initial height of the sample is approximately 6.4 mm. Parameters of the simulated sand particles are summarized in Table 1. The base critical energy release rate serves the reference case for a particle with 1.6 mm diameter. The sample is packed by depositing a randomly generated particle cloud under gravity. Particles in the cloud are initially assigned with the same weak plane orientation. During the packing process, particles move and rotate which leads to diversified orientation of the weak plane among the particles. Load is applied at a rigid platen on the top of the sample to a maximum level of 22 MPa. The loading process is simulated with a total

Table 1 Summary of simulation parameters for the sand particles

Parameter	Value
Density (kg/m^3)[a,b]	2650
Young's modulus (GPa)[b]	100
Poisson's ratio[b]	0.15
Base critical energy release rate (J/m^2)[b]	60
Weibull modulus[b]	3.0
Inter-particle friction coefficient[a]	0.5
Restitution[a]	0.0

[a]The parameter is used in discrete modeling by NSCD
[b]The parameter is used for particle crushing simulation by PD

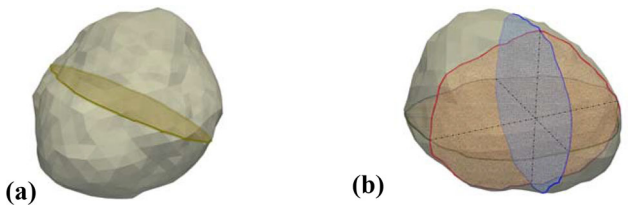

Fig. 6 Schematic illustration of modeled weak plane in particle: **a** single weak plane; **b** three orthogonal weak planes

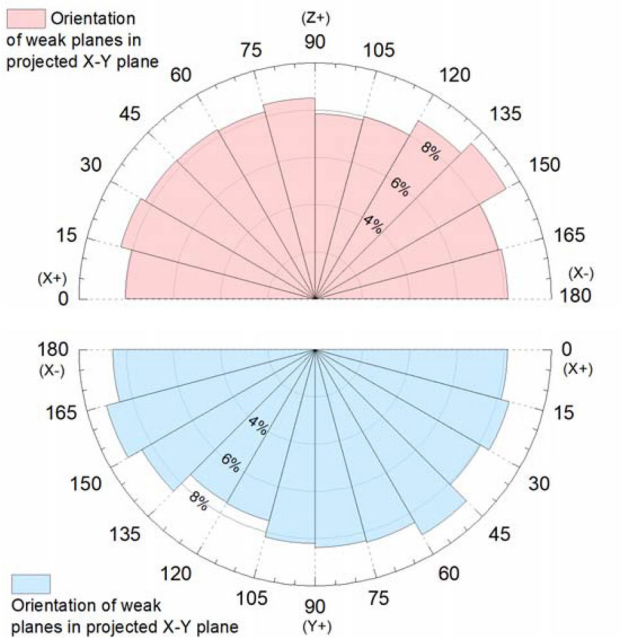

Fig. 7 Distribution of the normal direction of weak planes in all particles that experience crushing. The data are obtained from the simulation for the case where a single weak plane is modeled in all particles. The normal directions of the weak planes are projected on the x–z plane (upper half plot) and x–y plane (lower half plot). Radial length in the plot indicates the occurring probability on each direction. The angle (from 0 to 180 and in degrees) indicates deviation from positive x axis

number of 39,000 time steps in NSCD, where the time step size is 8×10^{-6} s before 20 MPa and 7×10^{-6} s afterward. Particle crushing is analyzed at a loading interval of about 0.09 MPa. A crushing limit is set at 0.3 mm, and particles with equivalent diameter smaller than that are assumed to be non-crushable.

Three cases are simulated. The first case, which serves as a reference case, only consists of isotropic particles, i.e., without plane of weakness. In the second case, one crossing weak plane is modeled in each particle. It represents structure of a single direction cleavage (e.g., in minerals like mica). In the third case, three orthogonal weak planes are modeled in each particle (e.g., in minerals with three orthogonal cleavage planes like halite). The two types of weak planes are illustrated in Fig. 6. For the latter two cases, it is intended to let the orientation of the weak plane distribute randomly among the particles so that the orientation itself does not play a significant role in particle crushing. This is achieved via two processes. One is the diversification in weak plane orientation during the packing process described earlier. The other is breakage of particles, after which the child particles move and rotate, leading to further diversification in the weak plane orientation. In fact, in the recorded particle crushing events, the weak plane orientation tends to be evenly distributed among all directions. This is demonstrated in Fig. 7 for the second case where a single weak plane is modeled in each particle. The normal directions of the weak plane for all particles that experienced crushing are plotted in a rose diagram, and a uniform distribution in all directions is evident.

3.2 Particle size and shape evolution

Snapshots of the simulated samples at the final loading stage are exhibited in Fig. 8. It is not surprising to observe that particles with weak structural planes experienced more severe fragmentation than those isotropic particles since the weak planes tend to reduce strength of the particles. The total number of particles during the loading process for the three simulated cases is shown in Fig. 9a. Apparently, samples with anisotropic particles exhibit quicker fragmentation. At the final loading stage, the number of particles for the three-weak-plane case is almost twice of that with isotropic particles. The observation can be attributed to two factors. One is that an individual particle tends to break into more fragments when weak planes are presented. Another is that more particles experienced breakage in samples with anisotropic particles. The two factors are confirmed in Fig. 9b: First, the average number of fragments in single particle breakage events for anisotropic particles is notably higher than that for isotropic particles. Second, more breakage events are seen in the anisotropic particles than in the isotropic particles. The total recorded number of particle breakage events is about 8500 for the three-weak-plane case, 7900 for the single weak plane case and 7200 for the sample containing isotropic particles.

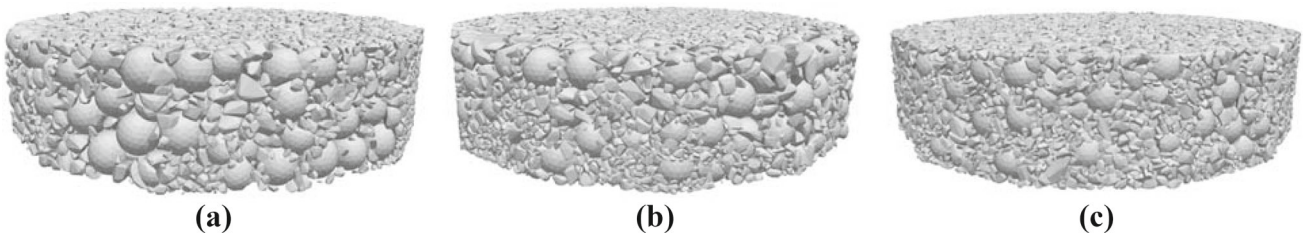

Fig. 8 Snapshots of the simulated sample at 22 MPa: **a** isotropic particles; **b** particles with single weak plane; **c** particles with three orthogonal weak planes

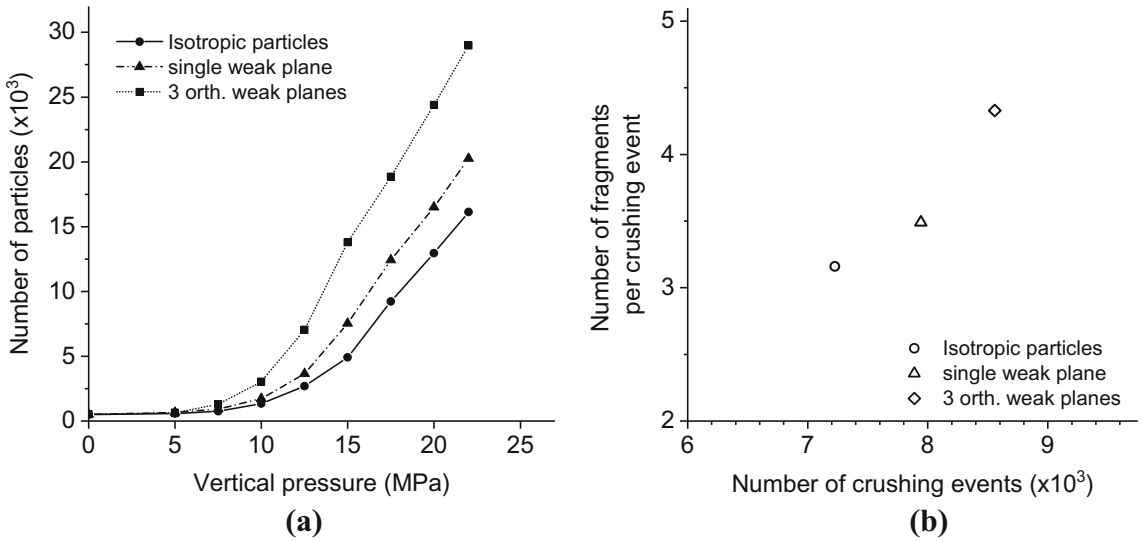

Fig. 9 Total number of particles in the simulation (**a**) and recorded particle crushing events and average number of fragments per crushing event (**b**)

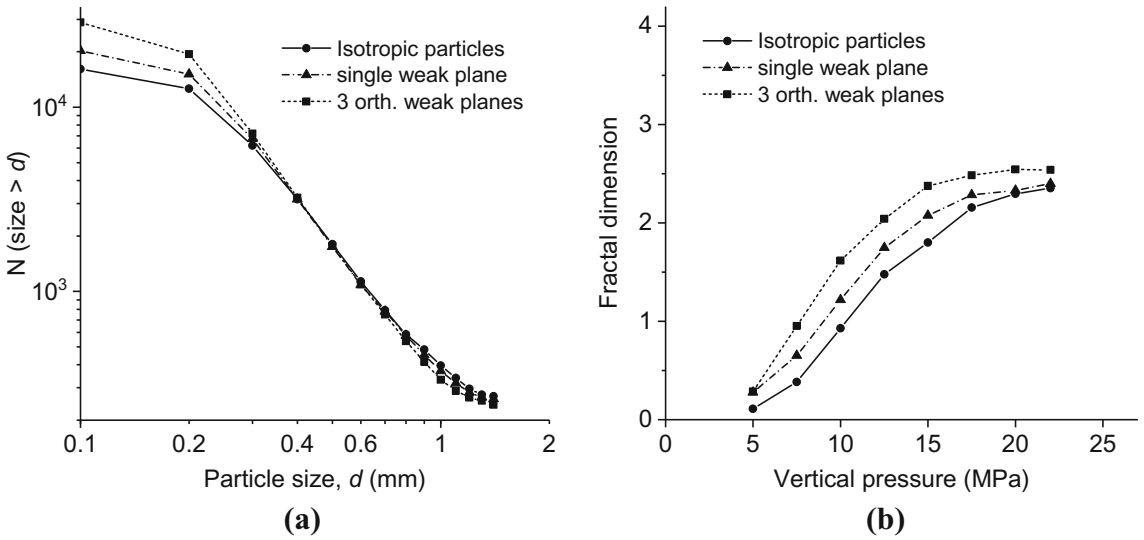

Fig. 10 Particle size distribution at final loading stage (**a**) and fractal dimension (**b**) obtained from simulation

Distribution of particle size resulted from fragmentation can be characterized using the concept of fractal [36], and many natural sands are found to have fractal dimensions between 2 and 3 [1, 37]. The fractal dimension is defined based on the slope of curve on a plot of particle size d versus the number of particles with size greater than d both in logarithm scale (Fig. 10a). For practical purpose, we select the portion of curve in the size range of 0.4 mm to 0.9 mm to

find fractal dimension. Other portions of the curves are not fractal due to the limited number of particles in large size range and a crushing limit set at 0.3 mm. Evolution of the fractal dimension for the three simulated samples is plotted in Fig. 10b. For all cases, the fractal dimension appears to evolve toward constant levels between 2.3 and 2.6. Particles with more weak planes exhibit slightly higher fractal dimension and faster evolution. This is consistent with a highly idealized theoretical model introduced by Palmer and Sanderson [38] where fractal dimension is expressed as a function of crushing probability and number of fragments. Higher crushing probability and more fragments per crushing (e.g., with more weak planes) lead to larger fractal dimensions.

Particle shape represents another important property of granular material. It is known to evolve with continuous grain crushing process, and the shape factors tend to achieve a steady state profile [39, 40]. Shape evolution for the anisotropic particles containing weak planes is examined here by reviewing shape factor distribution at different loading stages. Four shape factors are studied, which include sphericity, aspect ratio (AR), elongation index (EI) and flatness index (FI). Sphericity is defined as surface area of a sphere having the same volume divided by the surface area of the particle. The AR, EI and FI are calculated by S/L, I/L and S/I, respectively, where S, I and L represent the short, intermediate and long dimension of the studied particle calculated using principal axis approach. Figure 11 shows the particle shape evolution for the single weak plane case. Results for the three-weak-plane case are in a similar nature and are not shown for conciseness. It appears that all shape factors tend to evolve toward a steady state profile with increasing load. To examine the effect of weak plane on particle shape resulted from continuous crushing, the distributions of shape factors for the three cases at the final loading stage are plotted in Fig. 12. It indicates that, when weak planes are present, particles tend to be more elongated, flattened and less spherical. Such influence is most apparent with respect to sphericity and least significant with respect to flatness and elongation. It implies that the weak planes ease creation of new material surface with less energy consumption so that the fragments possess lower sphericity. Theoretically speaking, the weak plane may be expected to have significant influence on the shape of child particles depending on the loading direction. An example is shown in Fig. 3, where the child particles in Fig. 3b possess aspect ratios nearly twice of that in Fig. 3a when the loading direction changes from perpendicular to parallel to the weak plane orientation. Nonetheless, in the context of a granular system where particles are subject to multi-directional loadings and experience a continuous crushing process, such influence appears to be mitigated although notable differences in particle shape can still be observed. Another observation based on Fig. 12 is that particle shape distributions for the single weak plane case and three-weak-plane case do not seem to have significant difference. It implies that overall shapes of the fragmented particles are similar with different configurations of weak planes. The sphericity is nonetheless smaller when there are more weak planes which probably increases angularity of the fragments.

3.3 Particle strength and crushing energy

The strength of natural sand particles exhibits significant variance which can be statistically described by a Weibull distribution [41, 42]. Such characteristic of natural granular materials has been implemented in the presented simulations by statistically assigning critical energy release rate to the modeled particles with consideration of particle size effect [21]. Another important source of particle strength variation is attributed to particle shape. In this section, the particle shape–strength relationship is examined with consideration of the weak planes. The strength of a particle refers to the characteristic strength calculated by maximum normal contact force on a particle before crushing divided by square of equivalent diameter. The equivalent diameter is defined as the diameter of a sphere having the same volume to the particle. To ease comparison, the particle strengths are normalized by the strength of a spherical, isotropic particle having the same volume and critical energy release rate undergone diametrical compression. Such strength can be derived based on the size effect on particle strength and the relationship between particle strength and critical energy release rate, as presented in [21]. Sphericity is chosen herein as a representative particle shape factor. It is defined as the surface area of a sphere having the same volume to the particle divided by the surface area of the particle. The mean, median and range of particle strength in the three simulations are plotted against sphericity in Fig. 13.

Two major observations can be made. First, the existence of weak planes tends to reduce the shape effect on particle strength. In other words, particles with different shapes appear to have less strength variation if weak planes are present. For the modeled spherical particles containing single weak plane and three orthogonal weak planes, the mean strength is approximately 77% and 58% of that for isotropic particles, respectively. For those elongated or angular particles with sphericity less than 0.8, the mean strength for the single and three-weak-plane case is approximately 91% and 73% of that for isotropic particles, respectively. The weak planes appear to result in heavier strength reduction to the sphere-like particles than those with small sphericity. The observation may imply that, with more weak planes, crushing of a particle is increasingly dominated by the characteristics of weak plane (such as strength, location and orientation) rather than the shape of the particle. Second, for particles containing weak planes, the mean and median strengths remain

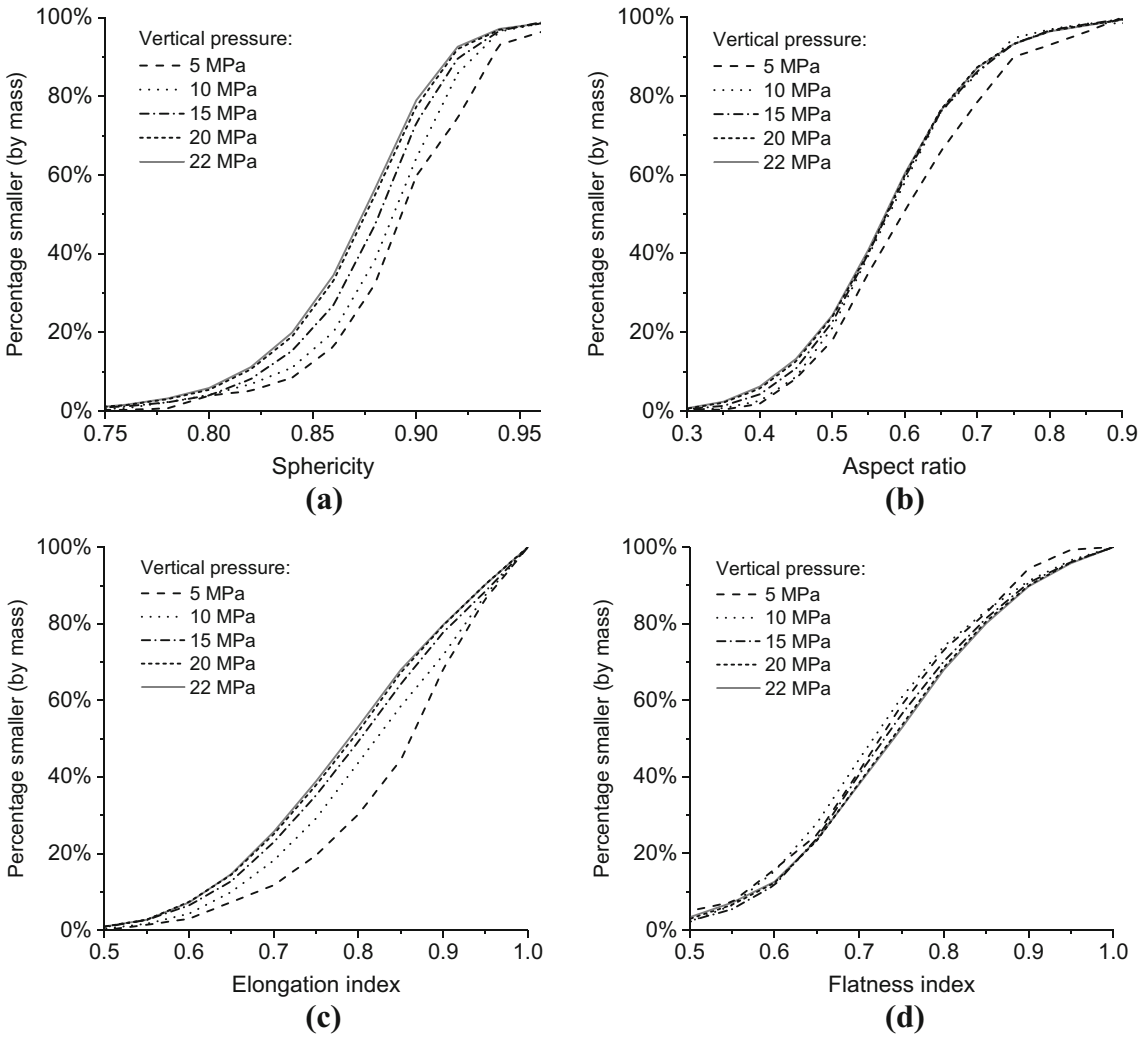

Fig. 11 Shape evolution due to continuous crushing process for particles containing single weak plane: **a** sphericity; **b** aspect ratio; **c** elongation index; **d** flatness index

approximately at the center of the strength range as reflected in Fig. 13. Since the strength is calculated based on maximum normal contact force on a particle, the results imply that a maximum-contact-force-based criterion continues to be valid as an approximate particle crushing criterion to be employed in simplified particle crushing models.

The specific crushing energy of particles, designated by the maximum strain energy per unit mass in the particle before crushing, in the three simulations is reviewed in Fig. 14. The specific crushing energy is normalized by specific crushing energy for a spherical, isotropic particle with the same volume and critical energy release rate and crushed under diametric load. Similar to the earlier observation, the existence of weak planes appears to mitigate particle shape effect on specific crushing energy. For spherical particles, comparing with the case with isotropic particles, the specific crushing energy exhibits a reduction of about 32% and 54% for the single and three-weak-plane case, respectively, whereas for particles with sphericity less than 0.8, such reduction is only 11% and 36%, respectively.

On macromechanical level, a yield stress, as defined at the point of maximum curvature of compression curve on a plot of void ratio versus logarithm of stress [43], is used to describe strength of granular media under one-dimensional compression. Yielding of granular material is a result of starting of significant particle crushing process [44], and the yield stress is therefore related to the strength of individual particles [43]. Compression curve and yield stress for the three simulated samples are examined in Fig. 15a. For the isotropic particles, yield stress is found to be 9.4 MPa. For particles containing single and three orthogonal weak planes, yield stress is approximately 8.7 MPa and 7.6 MPa, respectively, which represent a reduction of 7% and 20% from the case with isotropic particles. In comparison, the mean particle strength for samples containing single and three orthogonal weak planes is reduced by 17% and 32%, respectively. It

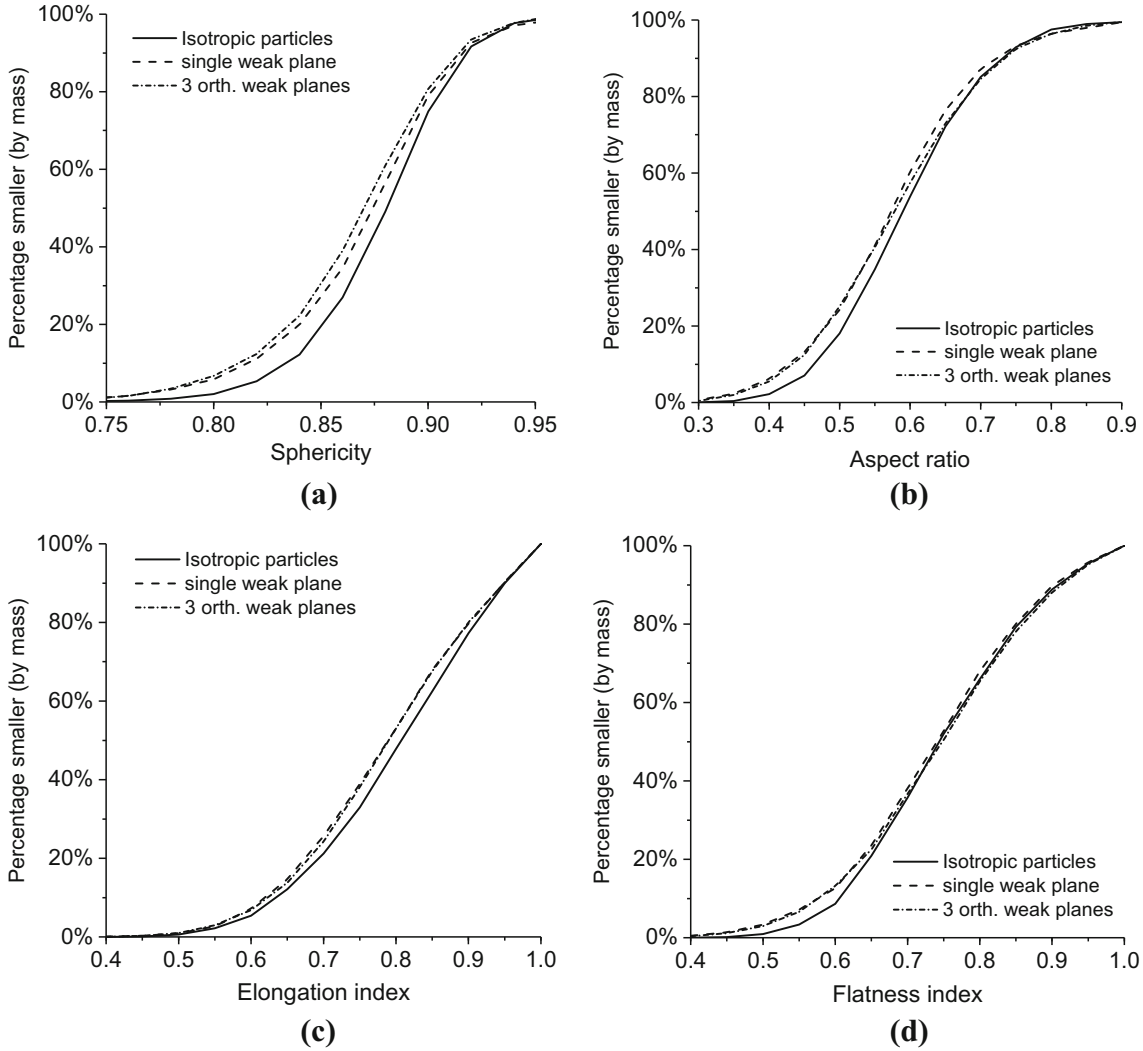

Fig. 12 Particle shape distribution at final loading stage for the three simulated samples: **a** sphericity; **b** aspect ratio; **c** elongation index; **d** flatness index

implies a monotonic but nonlinear relationship between the change in single particle strength resulted from microstructural weak planes and alternation in macroscopic yield stress. Probably, yielding of granular material is not solely depending on strength of individual particles but is also related to force distribution in the granular system, which further relates to particle-level morphology and crushing characteristics where the microstructural features play a role. Shown in Fig. 15b is the variation of compression index (C_c) during the loading process for the three simulated samples. The compression index refers to the absolute value of the slope of the compression curve. Variation of C_c with increasing load shows similar pattern comparing with experimental measurement [42] for uniformly graded sand, where C_c increases with load initially, reaching a maximum level, and decreases slightly afterward. As expected, rising of C_c is the earliest for particles containing three orthogonal weak planes, which tends to produce more and finer fragments. The maximum and post-peak values of C_c do not seem to have apparent difference among the three simulated samples.

We also examine the mean and deviatoric stresses in the sample during the fragmentation process. The two stresses, as denoted by p and q, respectively, are calculated by

$$p = \frac{1}{3}\sigma_{ii}, \quad q = \sqrt{3\left(\sigma'_{ij}\sigma'_{ij}\right)/2} \tag{7}$$

where σ represents the stress tensor and σ' is the deviatoric part of the stress tensor. σ is calculated following [45, 46] as

$$\sigma_{ij} = \frac{1}{V}\sum_{c\in N_c} f_i^c l_j^c \tag{8}$$

where f^c denotes force at contact c and l^c represents the branch vector connecting the centers of the contacting par-

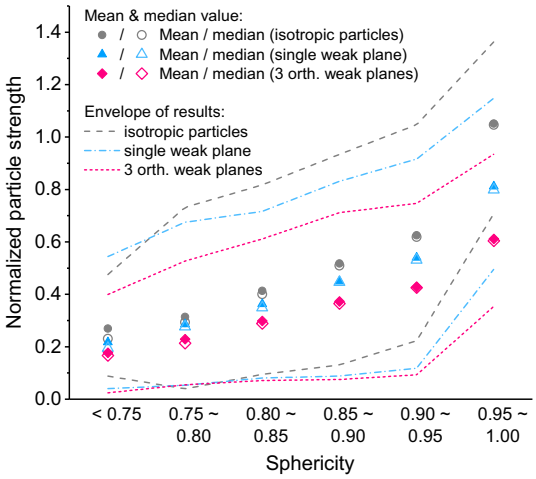

Fig. 13 Particle shape and strength relationship for the three simulated cases

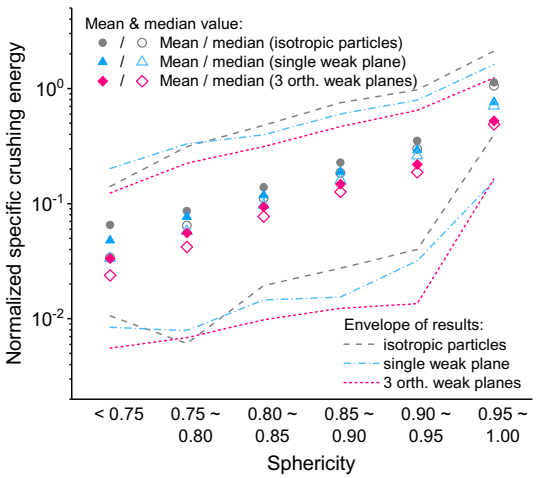

Fig. 14 Shape and crushing energy relationship for the three simulated samples

ticles. N_c is the total number of contacts in the sample. V is the volume of the sample. The shear strength of the three simulated samples, as denoted by a stress ratio of q/p, is plotted in Fig. 16a. The curve is potentially influenced by three underlying mechanisms. First, a more polydisperse gradation resulted from particle crushing tends to increase the shear strength [47]. Second, at early stage of particle crushing, the crushed particles are more angular than particles in the initial packing which are spherical, and shape-induced interlocking effect emerges and improves the strength. Third, finer particle size, as a result from continuous particle crushing, may reduce the macroscopic shear strength [47]. Under a confined condition, reduced particle size is known to render higher lateral earth pressure coefficient at rest [48] and, consequently, a decrease in q/p. Each of the three mechanisms may dominate at different stages of loading. At the beginning of compression, the stress ratio shows a spike at small volumetric strains, that is, when the particle crushing begins and the first two mechanisms are believed to dominate. The stress ratio is then maintained more or less the same for a certain loading period. The fluctuations in the curve are possibly due to the limited number of particles in the simulation and rapid alternation in the contact fabrics due to particle crushing. The curve exhibits a declining trend at large volumetric strain. At this stage, the third mechanism, which accounts for particle size reduction, is believed to dominate. Since the particles with three weak planes are found to crush into more and finer fragments (Fig. 9), it is not surprising to see the declining of the stress ratio starts earlier for that sample. The deviatoric stress q is plotted in Fig. 16b for the three simulated samples. Clearly, particles containing weak planes sustain less deviatoric stress and this again can possibly be attributed to the finer particles in those samples resulted from crushing. The difference between the deviatoric stress in those samples appears to be wider with progress of particle crushing.

4 Summary and conclusions

Presented in this paper is a numerical study on crushable granular materials with explicit consideration of particle-scale weak structural planes. The simulation approach is embedded in a multiscale modeling framework based on coupled PD and NSCD method. The weak planes in individual particles are modeled by setting a fraction of peridynamic bonds to be broken as an initial condition. Three cases are investigated for isotropic particles and anisotropic particles containing single and three orthogonal weak planes. The results are examined with respect to particle size and shape evolution, particle strength and crushing energy.

For anisotropic particles containing weak planes, particle crushing is characterized by a large number of fragments and a slightly higher fractal dimension. Particle shape factors including EI, FI, AR and sphericity are found to approach a steady state distribution with increasing load. The observation is similar to previous findings for isotropic particles. However, fragments of anisotropic particles exhibit different shape distributions which generally have smaller EI, FI, AR and sphericity. Particles with different configurations of weak planes do not appear to lead to large difference in the shape of fragments.

Strength and crushing energy of particles are known to be related to the shape of particles. Such relations are examined with consideration of the weak planes inside particles. It is found that existence of weak plane tends to mitigate the shape effect on particle strength and crushing energy. It is also suggested that maximum contact force remains a reasonable simplified criterion for estimating crushing condition for the anisotropic particles. Macromechanical yield stresses of the simulated samples are also examined. A monotonic relation-

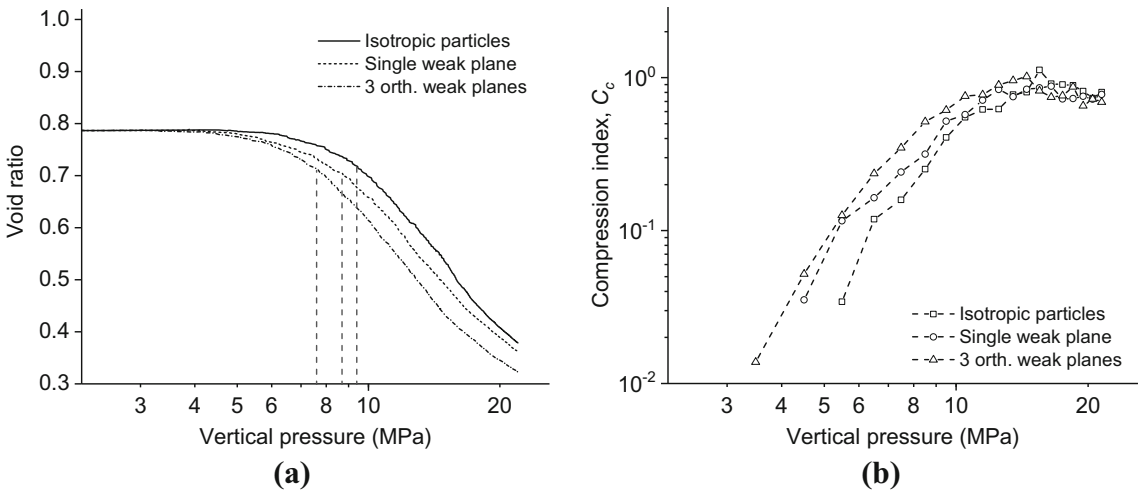

Fig. 15 **a** Compression curve of the three simulated samples and yield stress levels. The vertical dash lines indicate yield stress levels. **b** Compression index of the three simulated samples. The index is taken at every 1 MPa stress interval

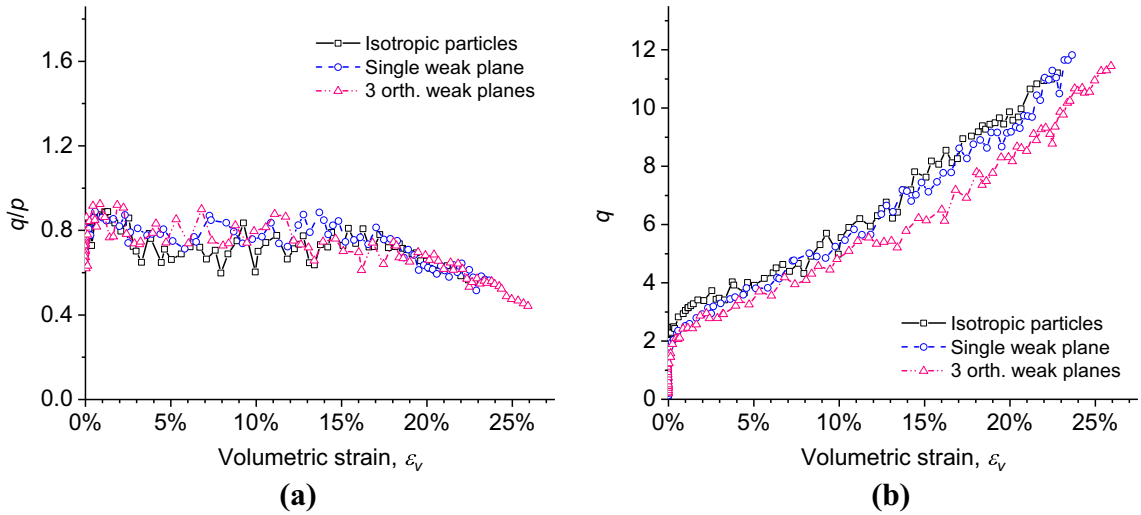

Fig. 16 Stress–strain relation of the three simulated samples during continuous particle crushing process: **a** ratio between the mean and deviatoric stresses versus volumetric strain; **b** deviatoric stress versus volumetric strain

ship is observed between particle strength and yield stress. The relationship appears nonlinear when alternation of particle strength is attributed to microstructural features. The microstructural features residing in particles are also found to affect shear strength of the sample, and the anisotropic particles appear less capable in sustaining deviatoric stress.

Acknowledgements The study was financially supported by the National Science Foundation of China under Project 11972030 and Research Grants Council of Hong Kong through GRF Project 16205418, 16201419, CRF Project C6012-15G and TBRS Project T22-603/15-N. The authors appreciate the constructive comments and suggestions offered by the anonymous reviewers.

Compliance with ethical standards

Conflict of interest The authors declare that they have no conflict of interest.

References

1. Zhao B, Wang J, Coop MR, Viggian G, Jiang M (2015) An investigation of single sand particle fracture using X-ray microtomography. Géotechnique 65(8):625–641
2. Altuhafi FN, Coop MR (2011) Changes to particle characteristics associated with the compression of sands. Géotechnique 61(6):459–471
3. Fonseca J, O'Sullivan C, Coop MR, Lee PD (2012) Non-invasive characterization of particle morphology of natural sands. Soils Found 52(4):712–722

4. Heng S, Guo Y, Yang C, Daemen JJK, Li Z (2015) Experimental and theoretical study of the anisotropic properties of shale. Int J Rock Mech Min Sci 74:58–68
5. Ma T, Peng N, Zhu Z, Zhang Q, Yang C, Zhao J (2018) Brazilian tensile strength of anisotropic rocks: review and new insights. Energies 11(2):304
6. Sadrekarimi A, Olson SM (2010) Particle damage observed in ring shear tests on sands. Can Geotech J 47(5):497–515
7. Cundall PA, Strack ODL (1979) A discrete numerical model for granular assemblies. Géotechnique 29(1):47–65
8. Jean M (1999) The non-smooth contact dynamics method. Comput Method Appl Mech Eng 177(3):235–257
9. Cheng YP, Nakata Y, Bolton MD (2003) Discrete element simulation of crushable soil. Géotechnique 53(7):633–641
10. Cil MB, Alshibli KA (2012) 3D assessment of fracture of sand particles using discrete element method. Géotech Lett 2(3):161–166
11. McDowell GR, Harireche O (2002) Discrete element modelling of soil particle fracture. Géotechnique 52(2):131–135
12. Lim WL, McDowell GR (2005) Discrete element modelling of railway ballast. Granular Matter 7(1):19–29
13. Nader F, Silvani C, Djeran-Maigre I (2017) Grain breakage under uniaxial compression using a three-dimensional discrete element method. Granul Matter 19:53
14. Nader F, Silvani C, Djeran-Maigre I (2019) Effect of micro and macro parameters in 3D modeling of grain crushing. Acta Geotech 14:1669–1684
15. Nguyen DH, Azéma E, Sornay P, Radjai F (2015) Bonded-cell model for particle fracture. Phys Rev E 91(2):022203
16. Cantor D, Azéma E, Sornay P, Radjai F (2017) Three-dimensional bonded-cell model for grain fragmentation. Comput Part Mech 4(4):441–450
17. Park B, Min KB (2015) Bonded-particle discrete element modeling of mechanical behavior of transversely isotropic rock. Int J Rock Mech Min Sci 76:243–255
18. Manouchehrian A, Sharifzadeh M, Marji MF, Gholamnejad J (2014) A bonded particle model for analysis of the flaw orientation effect on crack propagation mechanism in brittle materials under compression. Arch Civ Mech Eng 14(1):40–52
19. Munjiza A, Owen DRJ, Bicanic N (1995) A combined finite-discrete element method in transient dynamics of fracturing solids. Eng Comput 12(2):145–174
20. Ma G, Zhou W, Chang XL, Chen MX (2016) A hybrid approach for modeling of breakable granular materials using combined finite-discrete element method. Granul Matter 18(1):7
21. Zhu F, Zhao J (2019) Modeling continuous grain crushing in granular media: a hybrid peridynamics and physics engine approach. Comput Method Appl Mech Eng 348:334–355
22. Silling SA (2000) Reformulation of elasticity theory for discontinuities and long-range forces. J Mech Phys Solids 48(1):175–209
23. Silling SA, Epton M, Weckner O, Xu J, Askari A (2007) Peridynamics states and constitutive modeling. J Elast 88(2):151–184
24. Kilic B, Madenci E (2009) Prediction of crack paths in a quenched glass plate by using peridynamic theory. Int J Fract 156(2):165–177
25. Lai X, Liu L, Li S, Zeleke M, Liu Q, Wang Z (2018) A non-ordinary state-based peridynamics modeling of fractures in quasi-brittle materials. Int J Impact Eng 111:130–146
26. Zhu F, Zhao J (2019) A peridynamic investigation on crushing of sand particles. Géotechnique 69(6):526–540
27. Parks ML, Littlewood DJ, Mitchell JA, Silling SA (2012) Peridigm users' guide. Sandia report, Sandia National Laboratories, Albuquerque, NM, USA
28. Madenci E, Oterkus E (2014) Peridynamic theory and its applications. Springer, New York
29. Tavallali A, Vervoort A (2010) Effect of layer orientation on the failure of layered sandstone under Brazilian test conditions. Int J Rock Mech Min Sci 47:313–322
30. Mighani S, Sondergeld C, Rai C (2014) Efficient completions in anisotropic shale gas formations. In: Proceedings of the unconventional resources technology conference (URTEC), Denver, CO, USA
31. Tan X, Konietzky H, Frühwirt T, Dan DQ (2015) Brazilian tests on transversely isotropic rocks: laboratory testing and numerical simulations. Rock Mech Rock Eng 48:1341–1351
32. Saur H, Senechal P, Boiron T, Aubourg C, Derluyn H, Moonen P (2020) First investigation of quartz and calcite shape fabrics in strained shales by means of X-ray tomography. J Struct Geol 130:103905
33. Behzadinasab M, Vogler TJ, Peterson AM, Rahman R, Foster JT (2018) Peridynamics modeling of a shock wave perturbation decay experiment in granular materials with intra-granular fracture. J Dyn Behav Mater 4(4):529–542
34. Tasora A, Serban R, Mazhar H, Pazouki A, Melanz D, Fleischmann J, Taylor M, Sugiyama H, Negrut D (2016) Chrono: an open source multi-physics dynamics engine. In: Kozubek T (ed) High performance computing in science and engineering. Lecture notes in computer science. Springer, Berlin, pp 19–49
35. The CGAL Project (2017) CGAL user and reference manual, CGAL Editorial Board, 4.11 edn
36. Mandelbrot BB (1982) The fractal geometry of nature. W H Freeman and Company, New York
37. Turcotte DL (1986) Fractals and fragmentation. J Geophys Res 91(B2):1921–1926
38. Palmer AC, Sanderson TJO (1991) Fractal crushing of ice and brittle solids. Proc R Soc Lond Ser A Math Phys Eng Sci 433(1889):469–477
39. Ma G, Chen Y, Yao F, Zhou W, Wang Q (2019) Evolution of particle size and shape towards a steady state: insights from FDEM simulations of crushable granular materials. Comput Geotech 112:147–158
40. Ueda T, Matsushima T, Yamada Y (2013) DEM simulation on the one-dimensional compression behavior of various shaped crushable granular materials. Granul Matter 15(5):675–684
41. Nakata Y, Hyde AFL, Hyodo M, Murata H (1999) A probabilistic approach to sand particle crushing in the triaxial test. Géotechnique 49(5):567–583
42. Nakata Y, Kato Y, Hyodo M, Hyde AFL, Murata H (2001) One-dimensional compression behavior of uniformly graded sand related to single particle crushing strength. Soil Found 41(2):39–51
43. McDowell GR, Humphreys A (2002) Yielding of granular materials. Granul Matter 4(1):1–8
44. Hagerty MM, Hite DR, Ullrich CR, Hagerty DJ (1993) One-diensional high-pressure compression of granular media. J Geotech Eng 110(1):1–18
45. Christoffersen J, Mehrabadi MM, Nemat-Nasser S (1981) A micromechanical description of granular material behavior. J Appl Mech 48:339–344
46. Shi XS, Nie J, Zhao J, Gao Y (2020) A homogenization equation for the small strain stiffness of gap-graded granular materials. Comput Geotech 121:103440
47. Islam MN, Siddika A, Hossain MB, Rahman A, Asad MA (2019) Effect of particle size on the shear strength behavior of sands. Aust Geomech J 46(3):75–86
48. Wang JJ, Yang Y, Bai J, Hao JY, Zhao TL (2018) Coefficient of earth pressure at rest of a saturated artificially mixed soil from oedometer tests. KSCE J Civ Eng 22(5):1691–1699